Powder Technology 361 (2020) 499–506

Contents lists available at ScienceDirect

Powder Technology

journal homepage: www.elsevier.com/locate/powtec

Computational fluid dynamics modeling and laboratory analysis of aerosol particles' capture on thin swirling water film in a Vortecone

Ashish Ranjan Kumar *, Adam Levy, Anand Kumar, Steven Schafrik, Thomas Novak

Department of Mining Engineering, 504 Rose Street, University of Kentucky, Lexington, KY 40506, United States

ARTICLE INFO

Article history:
Received 16 November 2018
Received in revised form 19 July 2019
Accepted 25 November 2019
Available online 26 November 2019

Keywords:
Computational fluid dynamics (CFD)
Aerosols
Multi-phase flows
Free-surface modeling
Volume of fraction (VOF)
Cleaning efficiency
Pollutant cleaning

ABSTRACT

This study was conducted to look at a new use case for the Vortecone scrubber. A Vortecone is an inertial separator that utilizes the momentum of dust particles to promote their capture. The turbulent airflow forces the water supplied at the periphery to deform continuously, resulting in a rapidly swirling film on the Vortecone surface. The heavier dust particles are differentially shed from the bulk airflow towards the vortex chamber surface where they are captured by the running water film. The Vortecone surface serves as the filter element. The authors use computational fluid dynamics to model the multiphase flow and particle transportation inside the Vortecone. Laboratory experiments using coal dust show the Vortecone to capture about 73% and 97% of particles exceeding 2.9μm and 5.9 μm at 0.28 m^3/s. The cleaning improves to 89% and 99% at the airflow of 0.38 m^3/s.

1. Introduction

Suspended particulate matter have diverse generation, shape, size, and transportation characteristics. Epidemiological studies, including chronic exposure studies, have indicated that their inhalation could be detrimental to human health [10]. Outdoor air pollution and prolonged exposure to particulate matter like dust in high exposure occupations including mining and construction activities could contribute to the onset of irreversible ailments like asbestosis, silicosis, and other diseases in personnel [2]. Researchers have identified the sources of respirable quartz and silica in underground coal mines and have shown that the presence of mineral matter has significant implications on lung tissues [21] [22]. Agencies like the Occupational Safety and Health Administration (OSHA) and the Mine Safety and Health Administration (MSHA) [25] promulgate policies that prescribe remedies to minimize the exposure of workers. These include specifying airflow requirements to dilute detrimental aerosols to harmless levels, prescribing wet-head cutting tools, isolating personnel, and numerous other measures including using a variety of dust scrubbing systems. Scrubbers contribute to productivity by ensuring a comfortable environment in addition to supporting compliance efforts with the mandated dust regulations.

A special class of scrubbers called flooded-bed dust scrubbers are installed on coal mining machines, called continuous miners, that operate in blind headings [11]. These scrubbers use porous fibrous type screens flooded with water sprays, as the filter element. However, these scrubbing systems require frequent maintenance because oversized particles are drawn into the inlet and clog the screen. Accumulation of coal particles on the screen reduces the rated airflow and the dust-capture efficacy of the scrubber, thereby exposing the machine operators to elevated levels of dust [7]. To address the issue of scrubber availability the authors investigated novel scrubbing techniques including inertial separators with multiple stages [15] that could capture a significant portion of dust while eliminating the frequent need for maintenance. Cyclone scrubber which now are indispensable to mineral processing industries were also studied [5,12].

A Vortecone scrubber is a system that uses the inertia of the particles for classification based on their mass and momentum. This inertial separator was invented at the Institute of Research for Technology Development, University of Kentucky to address a unique problem of capturing paint particles on automobile assembly lines. Only about 30–50% of the particles stay on the surface of the vehicles, resulting in large amounts of over-sprayed particles (European Patent Application. Patent No. EP 1 258 294 A2, 2002). A Vortecone as shown in Fig. 1 showed capture efficiencies exceeding 99.6%, in addition to reducing energy consumption by about 30%. Dust-laden air is brought in the Vortecone and water is supplied at the periphery of the same inlet. The fluids are accelerated towards the vortex chamber to produce complex swirling patterns in this multi-phase system [27]. The classical Rayleigh-Taylor instability of fluid interfaces leads immediately to a highly unsteady turbulent circulating flow pattern [13,23]. This vortex motion casts out the particles differentially based on their masses. The

* Corresponding author.
E-mail addresses: ashi.ismd@gmail.com, ashish.kumar@uky.edu (A.R. Kumar).

https://doi.org/10.1016/j.powtec.2019.11.093
0032-5910/

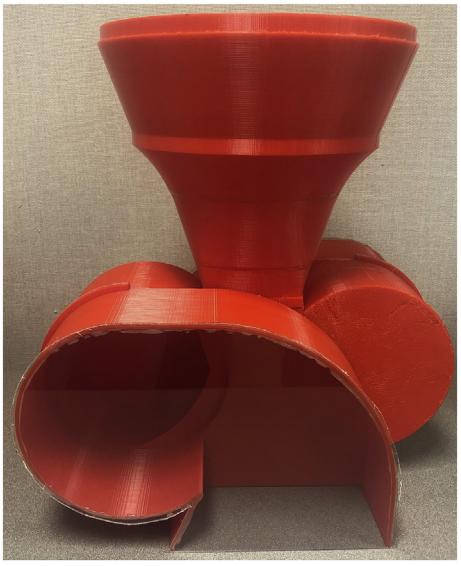

Fig. 1. A model of the Vortecone developed at the Institute of Research for Technology Development, University of Kentucky

shed particles travel towards the vortex chamber periphery and are trapped by the water film. Being a self-cleaning system, its availability is expected to be high even in hostile environments.

Computational fluid dynamics models were set up before initiating laboratory testing to estimate the operational parameters. Pressure drops and power requirements for known airflows were estimated through steady-state models. Transient-state simulations showed the development of free-surfaces in the Vortecone and the particle capture mechanism. The volume-of-fraction (VOF) technique was used to model the air-water interfaces in the transient-state simulations [4,9]. Following the usage of reduced scale models in dust mitigation studies earlier, a small-scale physical model was chosen for the ease of fabrication and testing for this research [3]. The following sections present the dust-capture results from the multi-phase CFD models generated to mimic the motion of thin water film under the combined effects of centrifugal forces, gravity, and surface tension, and the experimental results that validate the CFD models.

2. Computational fluid dynamics modeling

CFD is a finite volume method where numerical integration of Navier-Stokes equations for continuity, momentum, and energy conservation is carried out over the defined control volumes. Mass, momentum, and energy conservation equations have been shown below in Eqs. (1), (2), and (3), where ρ, μ, p, and β represents the fluid density (kg/m^3), viscosity coefficient (Pa.s), pressure (Pa), and coefficient of volume expansion (1/K) respectively. The parameter u_i represents the velocity component (m/s) along x_i-axis, t is the time (s), K represents the thermal conductivity (W/(mK))and T indicates the temperature (K). The term $\dot{e}$ represents the heat source (W/m^3).

$$(\partial u\_i)/(\partial x\_i\ ) = 0 \tag{1}$$

$$(\partial \rho u\_i)/\partial t + (\partial u\_j\ \rho u\_i)/(\partial x\_j\ ) = -\partial p/(\partial x\_i\ ) + \partial/(\partial x\_j\ )\mu((\partial u\_i)/(\partial x\_j\ ) + (\partial u\_j)/(\partial x\_i\ )) - \rho g\_i\ \beta(T - T\_o) \tag{2}$$

$$(\partial \rho C\_p\ T)/\partial t + (\partial u\_j\ \rho C\_p\ T)/(\partial x\_j\ ) = -\partial/(\partial x\_j\ )\ K\ \partial T/(\partial x\_j\ ) + \dot{e} \tag{3}$$

The software scFLOW, version 14, was chosen to develop the CFD models. The software uses polyhedral meshes and has independent modules for pre-processing, solving, and post-processing.

2.1. Pre-processing

A small physical model of the Vortecone used for research measured about 0.41 m × 0.36 m (height) × 0.32 m. A 3-D drawing of the Vortecone was generated first. The presence of symmetry about a vertical plane was utilized to bifurcate the flow domain of the simulations to save on computing resources. The geometrical features of the Vortecone were demarcated and assigned unique names in the software. An octree was then generated and refined preferentially to accurately capture the flow fields. Multiple layers of prisms were inserted on the impermeable surfaces to generate the computational mesh.

2.2. Steady-state simulations

Steady-state simulations were first generated using incompressible air at 20 °C as the working fluid to examine the behavior of flow patterns. Density was assumed to be 1.206 kg/m^3 and viscosity was assigned a value of 1.83E-05 Pa-s. Realizable k-ė, Spallart-Allmart, and RNG-k-é models are the most suitable turbulence models given their good abilities to represent these classes of flows accurately [26]. Realizable k-ė turbulent model was chosen since it yields good results with swirling flows and high-pressure gradients [1]. The boundary conditions involved a volumetric flow rate of 0.38 m^3/s at the inlet with associated turbulence kinetic energy and dissipation rates being 0.06 m^2/s^2 and 0.13 m^2/s^3 respectively. Suitable wall functions on the impermeable surfaces were imparted. The accuracy of time derivative terms was set at second order. All steady-state simulations converged with the residual threshold set at 0.0001 for the magnitude of velocities in three directions and the pressure.

Variation in velocity magnitude, Φ, at three points for the airflow of 0.38 m^3/s , when the solver converged according to the set criteria, was chosen as the parameter for mesh independence studies. These points were chosen close to the guide flaps of the inlet, close to the first curve at the bottom, and on the far-right surface of the vortex chamber, the locations being important for flow characterization. Richardson's extrapolation method of estimation and reporting of discretization errors was adopted [6,19]. The representative values of grid sizes, h_i, were first calculated for three different meshes, using Eq. (4a), where $h_1 < h_2 < h_3$.

$$hi = \left[\frac{1}{N}\sum_{i=1}^{N}(\Delta Vi)\right]^{1/3} \tag{4a}$$

Meshes were generated with a grid refinement factor, r_i, being the ratio of successive grid sizes, set at about 1.3.

Also, $r_{21} = h_2/h_1$ and $r_{32} = h_3/h_2$

An apparent order, p, was computed using Eq. (4b),

$$p = n1/\ln(r21)\ [\ln|e32/e21| + q(p)\ ] \tag{4b}$$

where $e_{32} = \Phi_3 - \Phi_2$ and $e_{21} = \Phi_2 - \Phi_1$

Eqs. (4c) and are used to compute intermediate values.

$$q(p) = \ln\{((r21)^p - s)/((r32)^p - s)\} \tag{4c}$$

and,

$$s = \ \text{sign}(e_{32}/e_{21}) \tag{4d}$$

Extrapolated values of the parameters, Φext_{21} and Φext_{32} were calculated using Eq. (4e),

$$\Phi\ ext^2 1 = \left(\left(\left(\Phi 1.r21^{((p)\ )} - \Phi 2\right)\right)/((r21^p - 1)\ )\right) \tag{4e}$$

Computed approximate and extrapolated relative errors, and the fine grid convergence index, GCI_{fine}, have been reported in

Table 1
Mesh parameters and values for the grid independence studies.

Parameter	Unit	Mesh 1	Mesh 2	Mesh 3
Number of elements, N	Number	426,171	1,025,746	2,346,437
Representative cell, h	mm	3.18	2.37	1.80
Velocity, Φ_1	m/s	33.46	32.51	32.45
Velocity, Φ_2	m/s	64.16	63.46	63.65
Velocity, Φ_3	m/s	63.44	62.61	62.60

Table 2
Discretization errors in CFD for the steady state airflow of 0.38m^3/s.

Parameter	Symbol	Φ_1	Φ_2	Φ_3
Approximate relative errors (%)	e_a^{21}	0.18	0.30	0.02
	e_a^{32}	2.92	1.10	1.33
Extrapolated values of velocities (m/s)	Φ_{ext}^{21}	32.45	63.73	62.60
	Φ_{ext}^{32}	32.45	63.19	62.60
Fine grid convergence index	GCI_{fine}^{21}	0.02	0.16	0.00
	GCI_{fine}^{32}	0.25	0.54	0.02

Tables 1 and 2. All these parameters were calculated using the MS Excel Solver. The values indicate good grid-independence; the mesh with about 1.02 million elements was chosen for further analysis. Transient state simulations depicting free-surfaces and particle transportation were then set up. Steady-state simulations with compressible air indicated negligible temperature change, incapable of influencing the existing phases of the fluids and hence the numerical captures. All simulations were, therefore, run with incompressible fluids to save additional computations on temperatures. Fig. 2 shows the mesh with 1.02 million elements which was used for all simulations further. Fig. 3 shows the contours of velocity magnitude from the converged steady-state simulation for the airflow of 0.38 m^3/s. CFD models are calibrated and their accuracy established using laboratory experiments [18]. A system curve showing pressure drops against flows was then plotted and would later be compared to the laboratory experiments.

2.3. Transient state simulations

The flow inside the Vortecone could be best modeled as an unsteady turbulent transient-state process. The number of inner iterations per cycle of calculations was set at 5 for all the transient state models depicting air-water interface and particle transportation.

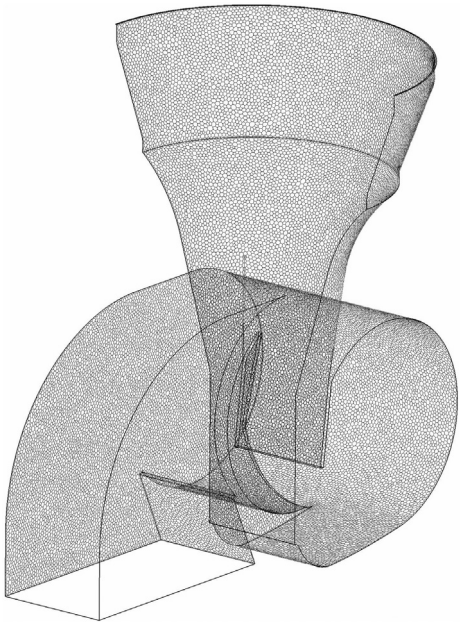

Fig. 2. The mesh with 1.02 million elements used for all simulations

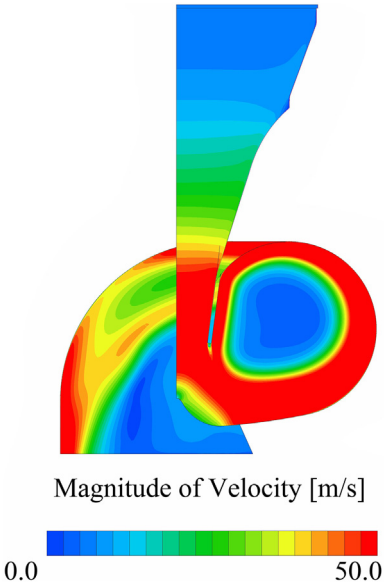

Fig. 3. Contours of velocity colored by the magnitude, air is observed to accelerate at much higher speeds compared to the inlet

2.3.1. Free-surface modeling

The free-surfaces inside the Vortecone were modeled using the volume of fraction (VOF) approach. Pure water and dry air were assigned the values of 1.00 and 0.00 respectively. All fractional numbers indicate free-surfaces with the quantity of water dictated by the magnitude of the VOF. The surface tension of water was set at 0.0714 N/m.

The fluids moving inside the Vortecone are accelerated by the inherent design of the Vortecone. Water and air crisscross paths immediately after the flaps and move towards the vortex chamber generating unsteady turbulent flow patterns [13] [17]. Air being the lighter fluid also interacts with the water film as it jumps from the flaps onto the curved surface at the bottom. This leads to perturbations at the interface, which soon transitions into a highly turbulent flow. The fluctuating trends of average Courant number plotted in Fig. 4 for first 1.00 s of flow affirm the highly chaotic nature of flow in the multi-phase system. This also leads to fleeting shapes of the film. Fig. 5 shows the free-surfaces, represented by a VOF of 0.01 at four different instances for the flux of 0.28 m^3/s and 22.71 l/min. The fluctuations in interfaces are usually very rapid and difficult to observe in real time. Fig. 6 shows the contours

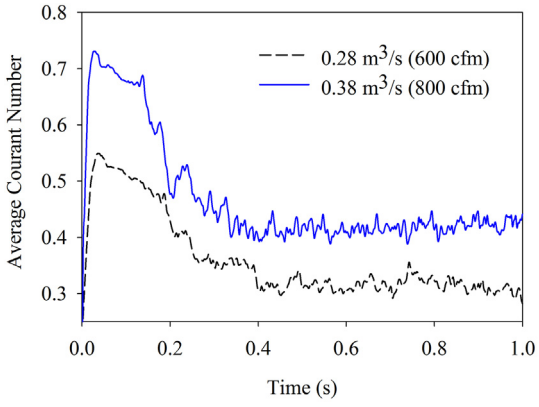

Fig. 4. Plot of time variation of the average Courant number for the two airflows for first 1.00 s

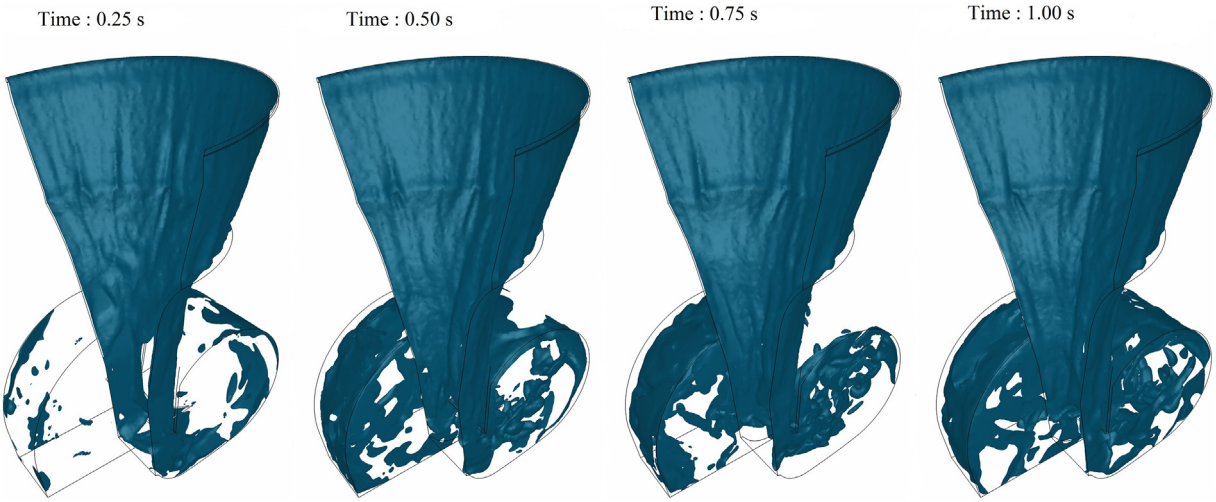

Fig. 5. Free-surfaces of the fluids, represented by a VOF value of 0.01 at different instances in time

of the velocity magnitude at four different instances. Spatial stability in their magnitudes is not achieved, long after the inflow and the outflow of fluids achieve equilibrium.

2.3.2. Particle tracking

Models to mimic the multi-phase flows of air and water were developed until 1.00 s when the inflow and the outflow rates of fluids moved towards an equilibrium. Beginning at the time, $t = 1.00$ s, perfectly spherical dust particles were randomly released at the Vortecone inlet every 0.5 ms continuously for next 0.25 s and tracked using the Lagrangian method. Drag force, F_D was computed on the particles every iteration using Eq. (4) shown here.

$$FD = CDX\ 0.5\ X\ \rho v^2 \tag{5}$$

where v is the relative velocity between fluid and particles, coefficient of drag, C_D is computed using Eq. (5) if Reynold's number, Re is less than 1000 and Eqs. (6a) and (6b) if it exceeds 1000.

$$CD = 24/Re(1 + 0.1255\ (\mathrm{Re})^{0.72}) \tag{6a}$$

$$CD = 0.44 \tag{6b}$$

The particle diameters ranged from 2.0 to 15.0 μm and were adopted from the characteristics of Keystone Mineral Black, 325 A, the coal dust sample used in the experiments. They were programmed to be destroyed at the outlet. The collision of the particles with the impermeable walls was assigned a coefficient of restitution of 0.95 to ensure that they are not trapped on the surfaces [24]. The diameters were adjusted using the corresponding Cunningham's slip correction factors [8]. A user-defined formatted script was compiled with the solver to track the particles that entered a mesh cell with a pre-assigned VOF. These particles were then stopped and their diameter set to 0.0 μm. Fig. 7 shows the particles in the Vortecone at the time, $t = 1.10$ and 1.20 s,

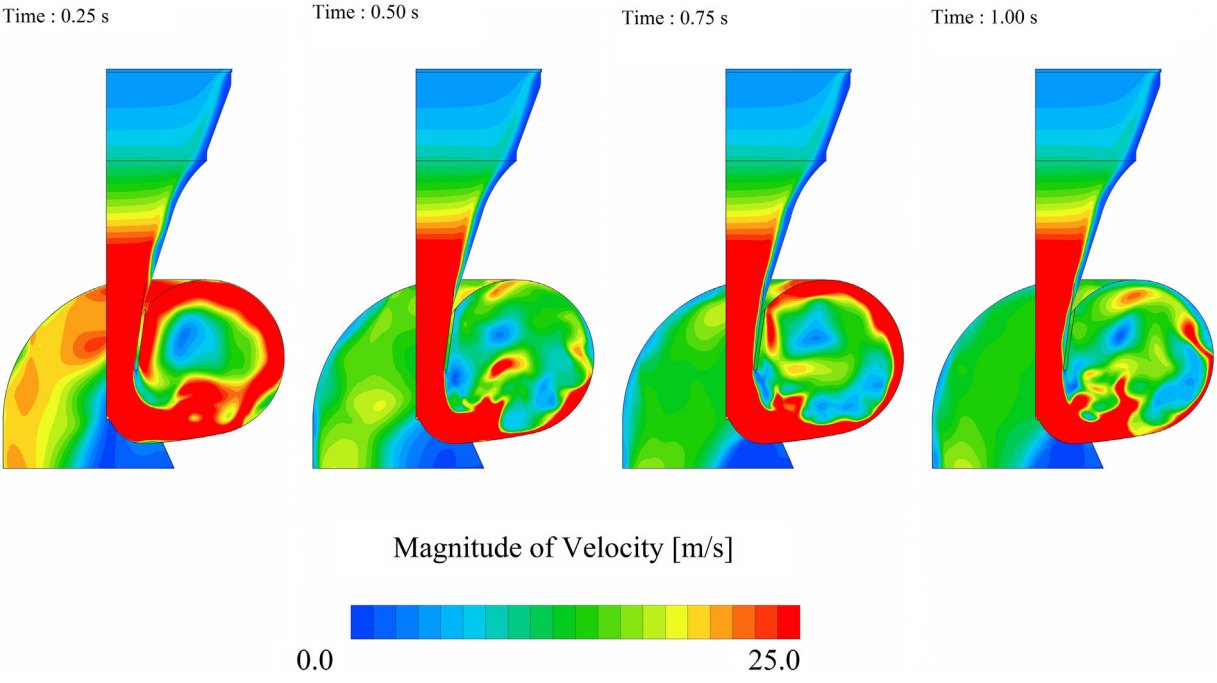

Fig. 6. Contours of velocity magnitude for the first 1.0 s of simulations on two parallel planes through the Vortecone

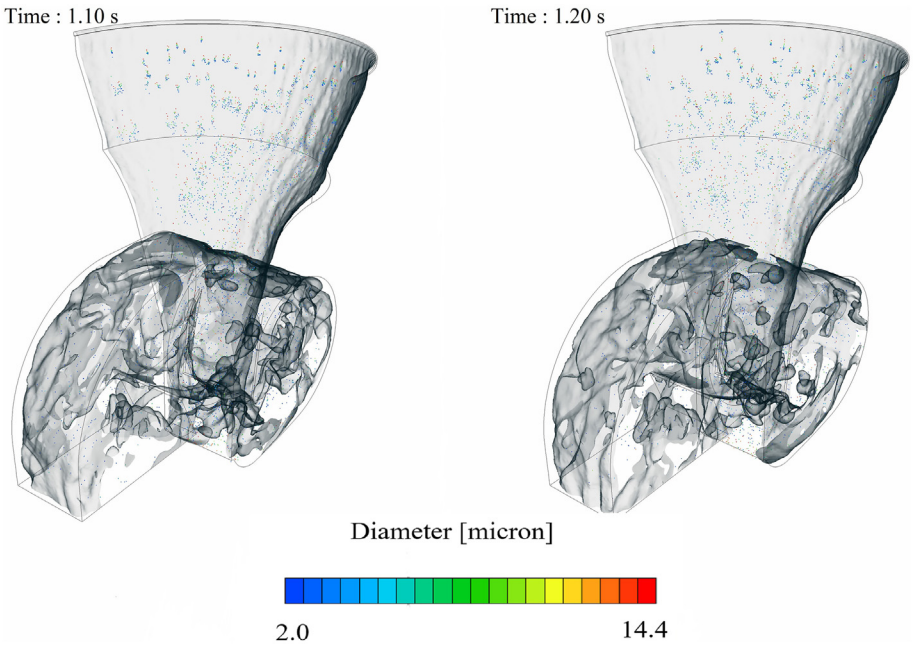

Fig. 7. Position of particles colored by their diameter, iso-surface of the interface has also been shown

Fig. 8. Construction of the Vortecone, flat transparent surfaces and water injection system shown

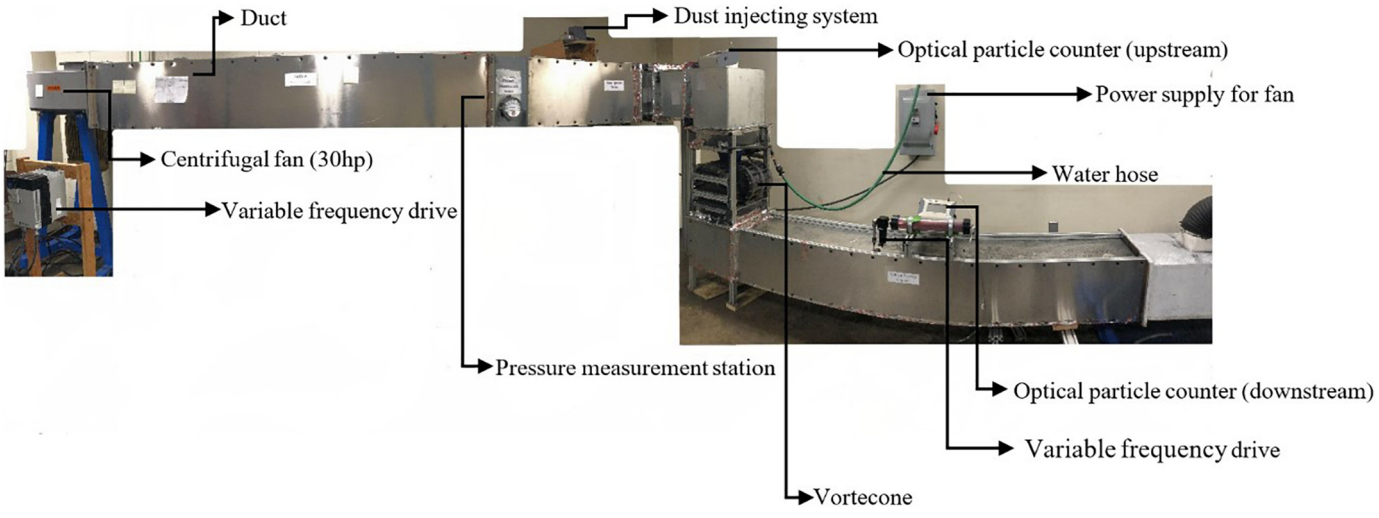

Fig. 9. Setup of the laboratory experiments

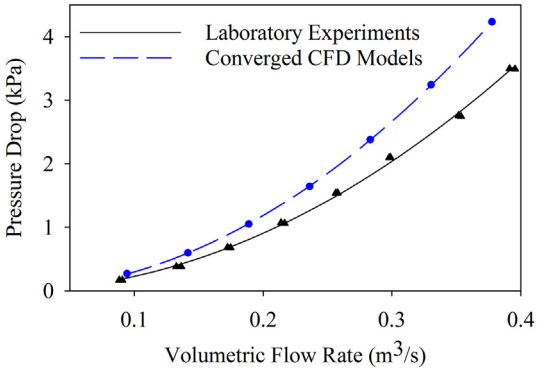

Fig. 10. Pressure-quantity curve of the Vortecone

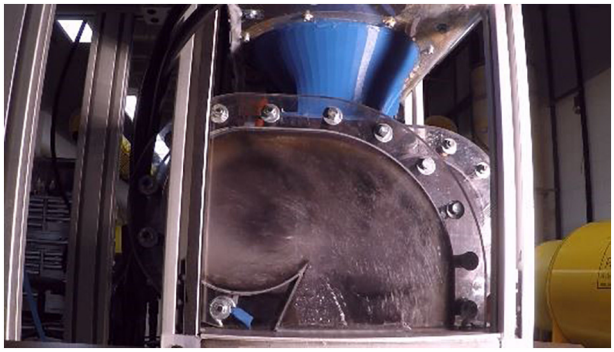

Fig. 11. Rapidly swirling film of water observed in the Vortecone for the airflow of 0.38 m^3/s and water inflow of 22.71 l/min

and colored according to their diameter magnitude. The particles were counted at the registered surfaces. At the time, $t = 1.50$ s, the number of particles reporting at the outlet was counted to estimate the number of particles trapped inside the Vortecone, and hence the cleaning efficacies.

3. Laboratory experiments

The following paragraphs describe the experimental set up to approximate the system curve and cleaning efficiency.

3.1. Description of experimental setup

Laboratory experiments were designed in the mine ventilation laboratory at the University of Kentucky to examine the performance of the Vortecone. A small-scale model was chosen for the ease of fabrication and testing [14]. The curved surfaces of the Vortecone were generated using a 3-D printer, whereas thick clear poly-carbonate sheets were used to construct the flat surfaces. The Vortecone was expected to be a high-pressure drop system. Therefore, duct-work serviced by a powerful centrifugal fan was designed and constructed to handle the high pressures. The cross-section of the duct-work measured 0.30 m × 0.48 m. Turning vanes were installed at the end leading into the Vortecone to cause a smooth transition of flow into the Vortecone. Honeycomb type flow straightener integrated pressure measurement station was installed downstream of the fan and upstream of the Vortecone to measure the total and static pressures. Fig. 8 shows the Vortecone during the assembly phase. Fig. 9 shows the experimental set-up with the Vortecone, the ductwork, and the fan. A circular channel was 3-D printed and four hoses connected to the laboratory water supply were attached at the periphery distributing the water evenly. The tests were run at a fixed water flow of 22.71 l/min and were kept constant through the course of the experiments.

3.2. Dust release and sampling

An auger feeder type dust induction station operating on laboratory compressed air was designed for a controlled release of Keystone mineral black- 325A dust into the pressurized duct. Identical TSI optical particle sizers (OPS 3330) were installed upstream and downstream of the Vortecone. Two and a half gram of coal dust was released into the duct over 4.0 min. This also ensured that the number of aerosol particles detected by the optical particle counter sensor is well under the maximum prescribed operational limits. To avoid under-sampling or over-sampling the airflow for the dust particles, isokinetic probes with the diameters sized appropriately were installed with their inlets positioned facing the airflow. The sampled air downstream was also led into a desiccant dryer to remove moisture before analysis by the OPS. The particles were then classified based on their diameters using the built-in software.

3.3. Experimental procedure

A multi-point traverse was first carried out across a plane, perpendicular to the airflow, 1.2 m from the outlet of the duct towards the Vortecone. The average velocity was compared to the readings obtained from the magnehelic and converted into the equivalent volumetric flow and was found to be in excellent agreement. Henceforth, the sensitive magnehelic was used to report the total and static pressures. The VFD frequency was first set at 10.0 Hz and then increased in steps of 5.0 Hz, and flow rates and pressure drops recorded. The steps were repeated three times to get a representative average. Fig. 10 shows the pressure-quantity curve for two sets of experimental trials, also called the system-curve. Good agreement was observed for the flow-rate pressure-drop plot between computer models and the experimental

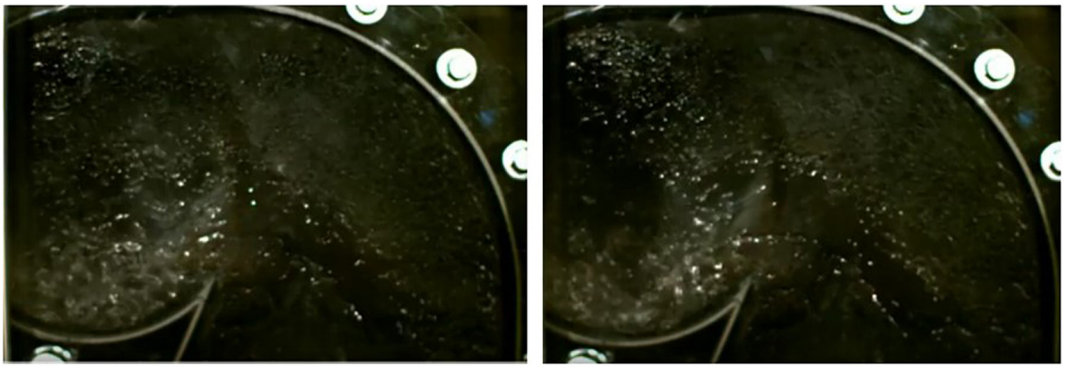

Fig. 12. Thin film shape captured by a high-speed video camera at different instances in time

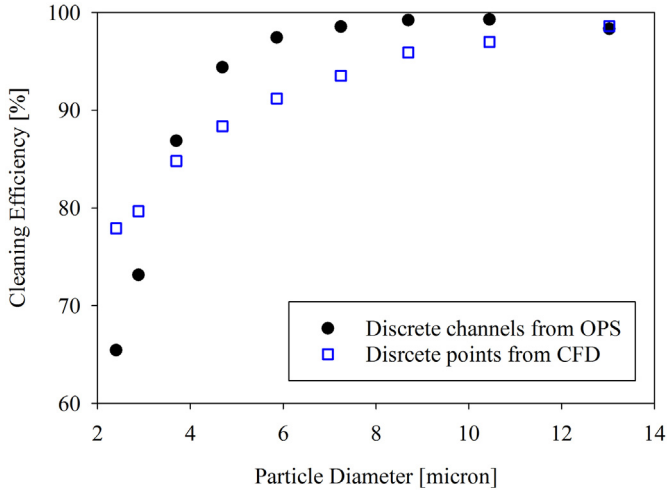

Fig. 13. Cleaning efficiency observed for the airflow of 0.28 m^3/s

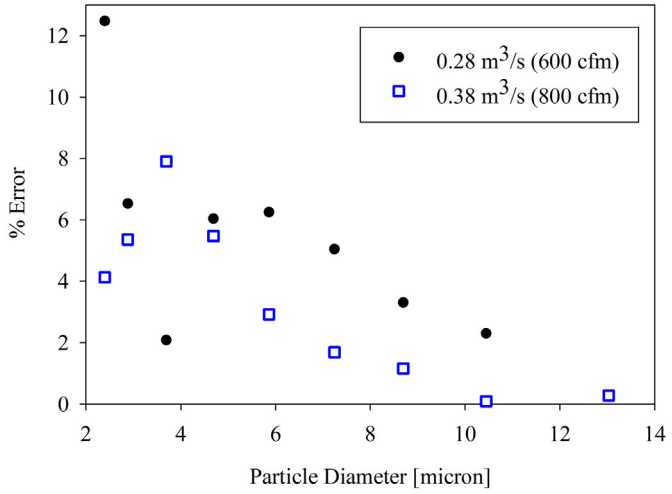

Fig. 15. The magnitude of percent errors between the laboratory test results and CFD models

data. The airflows also tend to follow the Atkinson's equation of ventilation [16].

Finally, the fan was run at fixed frequencies to yield average airflows of 0.28 m^3/s and 0.38 m^3/s in the ductwork. Airflow was sampled isokinetically at these flows and the particle count logged in the OPS. The number concentration was converted into mass concentration (observed to be of the order of mg/m^3 on both OPSs) using the Aerosol Instrument Manager software with the dead-time correction enabled. The difference in particle mass concentration recorded by the OPSs upstream and downstream of the Vortecone and averaged over three randomly designed runs indicated the cleaning efficiency for these flows. Fig. 11 shows the instantaneous shape of turbulent swirling film of water inside the Vortecone. The film is observed to drench most of the Vortecone surface. The film actively assists in particle removal and prevents build up. Fig. 12 shows the still images of the film recorded on a high speed camera. This shows the water distribution on the Vortecone surface at different instances, similar to CFD model predictions.

3.4. Results

The research examined the performance of a Vortecone scrubber for its ability to remove coal dust particles ranging in size 2.0–15.0 μm from airstream. Estimation of operation points of the Vortecone was also indispensable since this dictated the power requirements and operation costs. Results obtained from computer models and laboratory tests indicate excellent cleaning efficiency of the Vortecone. Figs. 13 and 14 show the mean cleaning efficiencies obtained from laboratory experiments and compared with the CFD modeling results for the increasing airflows. The experiments show that the Vortecone captures more than 73% of the dust-particles exceeding 2.8 μm in diameter and more than 97% of the particles exceeding 5.9 μm in diameter by mass at an airflow of 0.28 m^3/s. The cleaning efficiency is enhanced to 89% and 99% for the same particle size at a higher airflow of 0.38 m^3/s. The water inflow was kept constant at 22.71 l/min for all the tests. Average errors of 4.9% and 3.2% were observed between the CFD models and laboratory tests for airflows of 0.28 m^3/s and 0.38 m^3/s respectively. The errors have been shown in Fig. 15 and could be attributed to a variety of reasons including difficulty in sampling smaller aerosols. The cleaning efficiency increases as the size and mass of the particles increases. The larger particles have a more pronounced momentum and are more likely to get captured near the Vortecone curved surface which is the filter element. The water film trap and continuously remove the particles to eliminate build-up and filter clogging. The smaller particles tend to follow the streamlines, and hence do not impact the swirling surfaces of water and escape capture by the Vortecone.

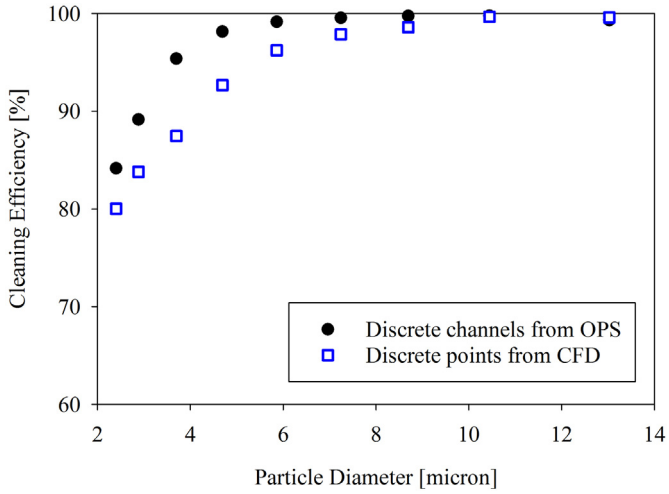

Fig. 14. Cleaning efficiency observed for the airflow of 0.38 m^3/s

4. Conclusions

The objective of this research was to determine if the Vortecone would be a suitable scrubber system for the rigors and dust generated by mining activities. This research examined the cleaning efficacies of the Vortecone wet scrubber system under conditions and airflows it was not originally designed to handle. Air and water traveling at high speeds inside the Vortecone give rise to instabilities immediately followed by unsteady turbulent flow, requiring CFD models to estimate the operation parameters. This testing indicated the Vortecone is effective but has a high pressure drop. CFD also demonstrated the free surfaces of fluid interface inside the Vortecone, which has not been previously studied and indicated the critical areas of capture and pressure loss. Volume of fraction approach was adopted to represent the interface, this helped lower the computational resources requirement as well in addition to representing the fleeting thin films. User-defined formatted scripts were built into the program to numerically model particle capture on film surface.

CFD results are supported by laboratory experiments. The trend of operational parameters, including airflow quantities and particle captures obtained during the laboratory tests agree well with those of the

numerical models for all particle removal efficiency. Excellent cleaning efficiency of the Vortecone shows it to be suitable alternative filter for particle separation and dust cleaning applications.

Acknowledgment

The authors acknowledge the National Institute for Occupational Safety and Health (NIOSH) for funding the research via Grant 200-2014-59922- 'Coal Mine Dust Mitigation through Novel Scrubber Development and Numerical Modeling.' This work is directed towards alleviating the onset of irreversible and often fatal diseases like coal workers pneumoconiosis (CWP) in underground miners. The authors acknowledge Dr. Kozo Saito of the Department of Mechanical Engineering at the University of Kentucky and Dr. William Chad Wedding for their support and recommendations.

References

[1] A. Bakker, Computational fluid dynamics, Course Materials, Dartmouth College, 2006.
[2] R. Bascom, P.A. Bromberg, D.A. Costa, R. Devlin, D.W. Dockery, M.W. Frampton, M. Utell, Health effects of outdoor air pollution, Am. J. Respir. Crit. Care Med. 153 (1996) 3–50.
[3] J.A. Breslin, A.J. Strazisar, Dust-control strategies using scale models of coal mine entries and mining machines, Bureau of Mines, United States Department of the Interior, Pittsburgh Mining and Research Centre, Pittsburgh, PA, 1976.
[4] C.W. Hirt, B.D. Nichols, Volume of fraction (VOF) Method for the Dynamics of Free Boundaries, J. Comput. Phys. 39 (1981) 201–225.
[5] A.B. Cecala, A.D. Brien, J. Schall, J.F. Colinet, W.R. Fox, R.J. Franta, et al., Report of Investigation 9689, Dust Control Handbook for Industrial Minerals Mining and Processing, Centers of Disease Control and Prevention, Department of Health and Human Services, Pittsburgh, PA, 2012 Spokane, WA: National Institute for Occupational Safety and Health.
[6] I.B. Celik, U. Ghia, P.J. Roache, C.J. Freitas, H. Coleman, P.E. Raad, Procedure for estimation and reporting of uncertainty due to discretization in CFD applications, *J. Fluids Eng.* (2008, July 22) https://doi.org/10.1115/1.2960953.
[7] J.F. Colinet, W. Reed, J.D. Potts, Report of Investigation 9693, Impact on Respirable Dust Levels When Operating a Flooded-bed Scrubber in 20-ft Cuts, Centers for Disease Control and Prevention, Department of Health and Human Services, Pittsburgh, PA, 2013 Spokane, WA: National Institute for Occupational Safety and Health.
[8] E. Cunningham, On the velocity of steady fall of spherical particles through fluid medium, Proc. R. Soc. Lond. A 83 (563) (1910) 357–365, https://doi.org/10.1098/rpsa.1910.0024.
[9] V.R. Gopala, B.G. Wachem, Volume of fluid methods for immiscible-fluid and free-surface flows, Chem. Eng. J. 141 (2008) 204–221, https://doi.org/10.1016/j.cej.2007.12.035.
[10] M.R. Heal, P. Kumar, R.M. Harrison, Particles, air quality, policy and health, Chem. Soc. Rev. 41 (19) (2012, June 1) 6606–6630, https://doi.org/10.1039/c2cs35076a.
[11] F.N. Kissell, Information circular 9465, handbook for dust control in mining, National Institute for Occupational Safety and Health, Department of Health and Human Services, Centers for Disease Control and Prevention, NIOSH, Pittsburgh, PA, 2003.
[12] J. Krames, H. Buttner, The cyclone scrubber- a high-efficiency wet scrubber, Chem. Eng. Technol. 17 (1994) 73–80, https://doi.org/10.1002/ceat.270170202.
[13] H.J. Kull, Theory of Rayleigh-Taylor instability, Physics Reports 1991, pp. 197–325 , North-Holland https://doi.org/10.1016/0370-1573(91)90153-D.
[14] A.J. Levy, Laboratory Performance Comparision of Vortecone Intertial Dust Scrubber to Flooded-Bed Dust Scrubber, Thesis University of Kentucky, Department of Mining Engineering, Lexington, 2017 https://doi.org/10.13023/ETD.2017.106.
[15] V.A. Marple, K. Willike, Impactor Design, Atmos. Environ. 10 (1976) 891–896.
[16] M.J. McPherson, Incompressible flow relationships, in: M.J. McPherson (Ed.), Subsurface Ventilation Engineering, Springer, Netherlands, 1993 , Retrieved Dec 1, 2017.
[17] F.T. Nieuwstadt, B.J. Boersma, J. Westerweel, Stability and transition, in: F.T. Nieuwstadt, B.J. Boersma, J. Westerweel (Eds.), Turbulence: Introduction to Theory and Applications of Turbulent Flows, Delft, The Netherlands 2015, pp. 19–53, https://doi.org/10.1007/978-3-319-31599-7.
[18] W.L. Oberkampf, F.G. Blottner, D.P. Aeschliman, Methodology for Computational Fluid Dynamics Code Verification/Validation, 1998 26th AIAA Fluid Dynamics Conference. San Diego, CA.
[19] P.J. Roache, Perspective: a method for uniform reporting of grid refinement studies, J. Fluids Eng. 116 (1994) 405–413.
[21] S.J. Schatzel, Identifying sources of respirable quartz and silica dust in unnderground coal mines in southern West Virginia, western Virginia, and eastern Kentucky, Int. J. Coal Geol. 78 (2) (2009, April 1) 110–119, Retrieved from https://doi.org/10.1016/j.coal.2009.01.003.
[22] S.J. Schatzel, B.W. Stewart, A provenance study of mineral matter in coal from Appalachian Basin coal mining regions and implications regarding the respirable health of underground coal workers: A geochemical and Nd isotope investigation, Int. J. Coal Geol. 94 (2012, May 1) 123–136.
[23] D.H. Sharp, An overview of Rayleigh-Taylor instability, Physica 12 (1984) 3–18.
[24] C. Tsai, D. Pui, B. Liu, Capture and rebound of small particles upon impact with solid surfaces, Aerosol Sci. Technol. 12 (3) (1990) 497–507, https://doi.org/10.1080/02786829008959364.
[25] United States Department of Labor, MSHA, Federal Register, Final Rule, Retrieved Nov 30, 2017, from United States Department of Labor, 2014, May 1 https://arlweb.msha.gov/regs/fedreg/final/2014finl/2014-09084.asp.
[26] H.K. Versteeg, W. Malalasekera, Turbulence and its modelling, An Introduction to Computational Fluid Dynamics, Longman Scientific and Technical 1995, pp. 41–84.
[27] A. Vinokurov, S. Shtork, S. Alekseenko, Experimental study of processing vortex core in two-phase flow, EPJ Web of Conferences 92 02107 (2015), EDP Sciences 2015, p. 2015, https://doi.org/10.1051/epjconf/20159202107.